# Quantum blockade and loop current induced by a single lattice defect in graphene nanoribbons

Jie-Yun Yan,[1,*] Ping Zhang,[1] Bo Sun,[1] Hai-Zhou Lu,[2] Zhigang Wang,[1] Suqing Duan,[1] and Xian-Geng Zhao[1]
[1]*Institute of Applied Physics and Computational Mathematics, P.O. Box 8009, Beijing 100088, China*
[2]*Department of Physics, and Centre of Theoretical and Computational Physics, The University of Hong Kong, Pokfulam Road, Hong Kong, China*
(Received 27 October 2008; revised manuscript received 21 January 2009; published 4 March 2009)

We investigate theoretically the electronic transport properties in narrow graphene ribbons with an adatom-induced defect. It is found that the lowest conductance step of a metallic graphene nanoribbon may develop a dip even down to zero at certain values of the Fermi energy due to the defect. Accompanying the occurrence of the conductance dip, a loop current develops around the defect. We show how the properties of the conductance dip depend on the parameters of the defect such as the relative position and severity of the defect as well as the width and edges of the graphene ribbons. In particular, for metallic armchair-edges graphene nanoribbons, whether the conductance dip appears or not, they can be controlled by choosing the position of the single defect.

DOI: 10.1103/PhysRevB.79.115403 PACS number(s): 73.63.−b, 72.10.Fk, 73.22.−f

## I. INTRODUCTION

Graphene has attracted intensive interest recently because of its novel properties, such as the room-temperature quantum Hall effect[1,2] and the Dirac-equations-governed electrons.[3,4] Moreover the properties of the graphene nanoribbons[5] change notably due to various edges,[6] different symmetries,[7] constrictions,[8] and even controllable defects by irradiating the material with electrons and ions.[9–11] Any wanted structures could be achieved by engineering the graphene with the help of state-of-art fabrication technologies, which supports the graphene as a prospective candidate for significant applications in electronics- and magnetics-related devices.

Defects have been revealed to be an influential factor in determining the transport properties of structures in nanoscale. For example, it has been known that defects can reduce or totally block the quantum conductance in carbon nanotube.[12–14] Graphene could be regarded as an unrolled carbon nanotube, and hence the transport of graphene in the presence of defects is also an interesting problem. Actually, several kinds of defects in a single layer of graphene have already been paid attention to such as pentagon/heptagon defects,[15,16] vacancies,[17] adatoms,[18,19] substitution,[20] disorder,[21] and even combinations of some of them.[22]

Although the electronic energy-band structures and magnetic properties in the presence of defect have been investigated in both graphene and graphene ribbons, how these properties manifest in transport is still lacking in attention. Recently, it has been found that the interior pentagon/heptagon defects[16] or the defects, such as vacancies or disorder at the edges,[23] would lead to total quantum blockade in graphene nanoribbons at certain Fermi energies. However, how the quantum blockade is connected with the severity or the positions (not limited to the edges) of the defect and the size or the symmetry of the graphene nanoribbons is not so clear. As the adatom defect would not change the topological structure of graphene lattice to some extent, the connection between these factors and the defect can be unambiguously understood by comparing with the clean graphene system. As we will show, all these factors are really critical on the influence of the defect. Therefore, a careful study of the influence of the adatom defect on the transport properties of graphene nanoribbons is deserved.

In this paper, we investigate the electronic transport in narrow graphene ribbons in the presence of a single defect, which could be induced by the absorption of a hydrogen atom. The model of the defect is based on the *ab initio* calculation. We find that the conductance profile is greatly reshaped by the defect. Compared with the integer steps of perfect graphene nanoribbons, the conductance in the presence of a single defect drops even down to zero in the low-energy regime, leading to a transformation from metal to semiconductor. Accompanied by this global conductance blockade, a loop current builds up around the defect. The conductances of the defective graphene nanoribbons with different widths, edges, and positions of the defect are studied. We find that the conductance blockade and the coexistence of the loop current sensitively depend on the severity and relative position of the defect. For metallic armchair-edges graphene nanoribbons, whether the conductance blockade and the coexistence of the loop current develop or not, they could be controlled by the position of the defect.

## II. MODEL AND RESULTS

The transport properties in graphene ribbons under low bias voltages are governed by the $\pi$-bonded electrons, which are modeled by the tight-binding spinless Hamiltonian,

$$\mathbf{H} = -t\sum_{\langle i,j\rangle}(c_i^{\dagger}c_j + \text{H.c.}), \tag{1}$$

where $c_i^{\dagger}$ ($c_i$) creates (annihilates) an electron on the site $i$, $t$ is the nearest-neighbor hopping energy and is set as 2.7 eV in this paper. The distance between the nearest-neighbor carbon atoms is $a$ ($\sim$1.42 Å).

The conductance can be calculated by the Landauer-Buttiker formula based on the Green's function method.[24–27] The formalism separates the entire system into three parts: the central region and two leads. To mimic the transport

 

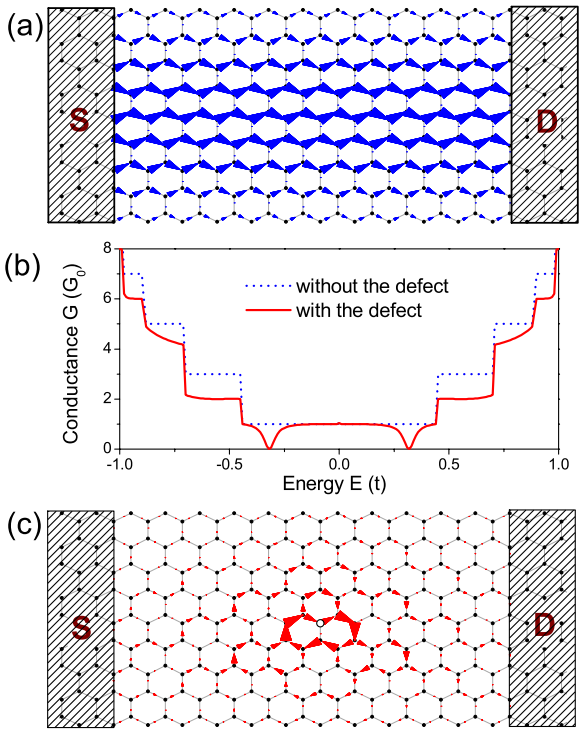


FIG. 1. (Color online) (a) The local electric current distribution in the perfect graphene ribbons. The sizes of the arrow represent the magnitude of the electric current between any two neighboring sites, which are linearly normalized to the maximum value. The source and drain are labeled with $S$ and $D$, respectively. (b) The conductances of a perfect graphene nanoribbon (dotted line) and the one with a defect (solid line). The position of the defect is shown in (c). (c) The local electric current distribution in the graphene nanoribbon with a defect marked by a hollow circle. The Fermi energy is $E=0.32t$.

through infinitely long ribbon with specific edge, two semi-infinite graphene leads are connected to the central region [see Fig. 1(a)]. The zero-temperature conductance $G$ of the graphene nanoribbons is given by $G(E)=\frac{2e^2}{\hbar}\mathrm{Tr}[\mathbf{\Gamma}_S(E)\mathbf{G}^r(E)\mathbf{\Gamma}_D(E)\mathbf{G}^a(E)]$, where $\mathbf{G}^{r(a)}(E)=[E\cdot\mathbf{I}-\mathbf{H}-\mathbf{\Sigma}_S^{r(a)}(E)-\mathbf{\Sigma}_D^{r(a)}]^{-1}$ is the retarded (advanced) Green's function matrix of the central part, $\mathbf{\Sigma}_{S(D)}^{r(a)}(E)$ is the retarded (advanced) self-energy due to the source (drain) [labeled as $S(D)$ in Fig. 1(a)], and $\mathbf{\Gamma}_{S(D)}(E)=i[\mathbf{\Sigma}_{S(D)}^r(E)-\mathbf{\Sigma}_{S(D)}^a(E)]$. Here $\mathbf{I}$ represents the unitary matrix. The local current density at the Fermi level $E$ between two neighboring sites $i$ and $j$ can be expressed as

$$i_{i\to j}(E)=\frac{4e}{\hbar}\mathrm{Im}[H_{ij}G_{ji}^n(E)], \tag{2}$$

where $\mathbf{G}^n=\mathbf{G}^r\mathbf{\Gamma}_S\mathbf{G}^a$ is the electron correlation function and $H_{ij}$ is the corresponding matrix element of the Hamiltonian.

In the absence of the defect, the well-known conductance of the perfect graphene nanoribbon with zigzag edges is shown by the dotted line in Fig. 1(b). Due to the metallic nature of the system, there exists no energy gap. The quantum conductance begins with $G_0$ (defined as $2e^2/\hbar$) and displays a typical step-increasing feature as a function of the Fermi energy. We also show in Fig. 1(a) the spatial distribution of the local current density at a selective energy value of $E=0.32t$. One can see that the current throughout the nanoribbon is uniform along the transport direction and forms unambiguous paths. At this energy, the current-density amplitude at the central region of the nanoribbon is bigger than that at the edge regions.

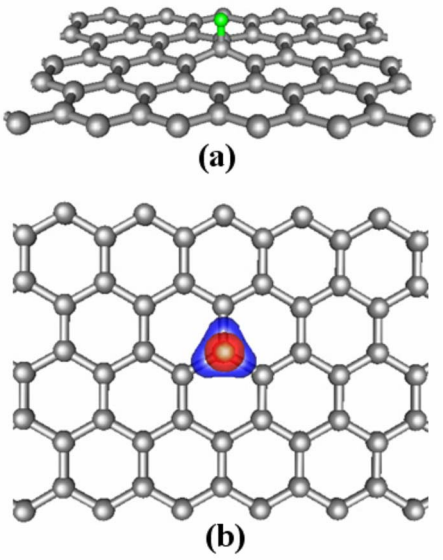


FIG. 2. (Color online) Adsorption of H on graphene: (a) the side view of H/graphene system with an H adatom (the small green ball) adsorbed at the on-top site of the graphene (the big gray balls). (b) The top view of the isosurface of the electron-density difference ($\pm 0.05e/\text{Å}^3$). Charge flows from the blue into the red regions.

Now, let us focus on the effect of a single defect site on the quantum conductance and local electric current distribution in the graphene nanoribbons. To physically illustrate how to model the presence of a single defect site by coupling a single carbon atom in the graphene with an adatom atop, we have simulated the atomic hydrogen adsorption on the graphene [see Fig. 2(a)] at a low coverage of 0.02 monolayer (namely, one hydrogen atom presents in a $5\times5$ graphene supercell) by using density-functional theory within the local-density approximation and a supercell approach. The total-energy calculation shows that the most stable adsorption site for H adatom is the on-top site and the H-C bond is characterized by a hybridization of H $1s$ and C $2p_z$ states. Prominently, it is found that the C atom beneath the H adatom is pulled a little bit out of the graphene plane by H-C chemical bonding, which obviously alters the coupling between this C atom and its three neighboring C atoms and thus results in a single lattice defect site. For further clarification, Fig. 2(b) plots the calculated electron-density difference $\Delta n(\mathbf{r})$, which is obtained by subtracting the electron densities of noninteracting component systems $n_{\text{graphene}}(\mathbf{r})+n_{\text{H}}(\mathbf{r})$ from the density $n(\mathbf{r})$ of the H/graphene system, while retaining the atomic positions of the component systems at the same location as in the H/graphene system. One can see that the charge redistribution only occurs around the H-C bond and influences the three neighboring C-C bonds, while the charge densities of other C atoms are not affected at all.

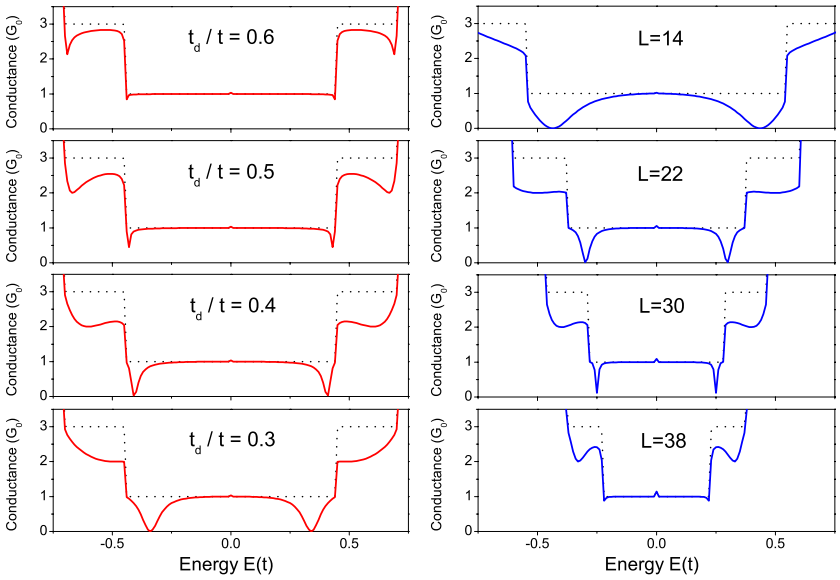


FIG. 3. (Color online) Left: conductances with the ratio $t_d/t$ decreasing from top to bottom. The system is the same one as in Fig. 1. Right: conductances of the graphene nanoribbons with different widths. In this case, the position of the defect and length of the ribbon is the same as the one in Fig. 1. The width changes by cutting or adding chains of C atoms at the bottom of the graphene nanoribbons. $L$ is number of the atoms connecting the source lead. For every plot, the conductance of the perfect graphene nanoribbon is shown for reference with the dotted lines.

Based on the physical picture revealed in Fig. 2, we model the presence of a single defect-lattice site by modifying the interactions between this lattice site and its nearest-neighboring sites while keeping other hopping elements unchanged. Therefore we change the hopping amplitude between the single defect site [hollow circle in Fig. 1(c)] and its three nearest neighbors from $t$ to, for example, $t_d=0.3t$. The conductance of the system with the defect is calculated and plotted with the solid line in Fig. 1(b). One can see that the conductance is prominently reshaped by the presence of the single defect site. The explicit changes include: (i) compared to the perfect case, the quantum step feature disappears; (ii) the conductance drops for most Fermi energies; and (iii) zero-conductance dips appear at certain Fermi energies. These defect-induced phenomena are understandable because the defect is a kind of destructive factor for the electron transmission in otherwise perfect graphene lattices. We now concentrate on the conductance dip at $E=0.32t$. Since the conductance drops to zero at this point, it means that the transmission is totally blockaded by the defect. The dip also implies the appearance of energy gap and consequently a transformation from metal to semiconductor happens. For further explanation to the conductance dip, we calculate the local current density at the Fermi energy ($E=0.32t$) and plot the result in Fig. 1(c). Compared to the ideal graphene nanoribbon system [Fig. 1(a), plotted at the same energy $E=0.32t$], it shows in Fig. 1(c) that the pattern of local current-density distribution is prominently changed in the defect-included system and there appears loop current circling around the defect site. The magnitude of this loop current around the defect can be larger than the maximal current in Fig. 1(a). Note that the current is normalized to the maximum value for each case. The loop current would produce an effective magnetic field, which is consistent with the previous experimental and theoretical predication.[17,18,28]

The formation of the loop current could be explained as the interference of all transport channels. In the two-dimensional graphene lattices, an electron could jump from source to drain via many different transport channels. The local electric current actually demonstrates the interference results of these channels. A defect would cause the blockade of relative transport channels to some extent and therefore change the local electric current. A discussion using a simple one-dimensional model is given in Ref. 23. As the different transport channels are numerous in the two-dimensional graphene lattices, whether the loop current appears and what kind of patterns it takes depend on the whole environment of the defect such as the edges and width of the graphene ribbons, the position and severity of the defect, etc. Therefore, we would dwell on the influence of these parameters on the transport properties in the defective graphene ribbons.

We can define the severity of the defect site by the ratio $t_d/t$. The vacancy defect is actually the defect with $t_d/t=0$. A question thereby arises. How effective could the defect cause the conductance to drop to zero? In the following, we will show that it depends on the competition between the width of the graphene ribbon and the severity of the defect. For a narrow graphene ribbon, the zero conductance exists in most cases when for small ratios of $t_d/t$. In the left panel of Fig. 3, we present the conductance of the same defective graphene ribbon as in Fig. 1 but with different $t_d/t$. We can see that as the ratio $t_d/t$ decreases, the dip begins to appear in the lowest conductance step and conductance reaches zero at $t_d/t=0.4$. This critical value at which zero conductance is obtained is also dependent on the width of the graphene ribbon. To show the influence of the width, we modify the width of the defective graphene nanoribbon shown in Fig. 1 by cutting or adding chains of C atoms on the lower edge of the ribbon. The width $L$ is denoted by the number of chains. In the right panel of Fig. 3, the conductances of the graphene ribbons with four different widths are plotted. It is obvious that as the width of the graphene ribbon gets wider, the dips become shallow and narrow and finally almost disappear. For the case of $L=38$, the values of conductances almost get equal between $E=0.22t$ and, for example, $E=0.1t$. However, the loop current only exists near $E=0.22t$ (not $E=0.1t$), although the net current cannot be totally blocked by the defect.

Besides the change in intersite hopping matrix elements by the coupling of a single lattice site with the adsorbed atom, the on-site energy of this lattice site may also be

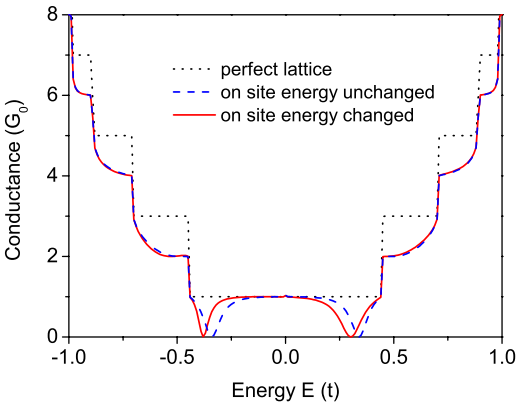


FIG. 4. (Color online) Conductance calculated for the case when the on-site energy of defect adds $0.1t$ shown with the solid line. Other parameters are the same as in Fig. 1(b). For reference, the case of a perfect lattice (dotted line) and the one with a single defect but assuming on-site energy unchanged (dashed line) are also shown.

changed due to the bonding and antibonding hybridizations. The conductance by changing the on-site energy of the defect site by $0.1t$ is shown in Fig. 4. We see that the conductance dip still appears but lies at a shifted energy not far away. The distance depends on the changed amplitude of on-site energy. At the conductance dip, the loop current also exists without apparent difference from the one shown in Fig. 1(c). So we conclude that the on-site energy is not an influential factor to the occurrence of conductance dip and formation of loop current induced by the single defect in this model.

We have also studied the influence of the position of the defect site on the conductance of the graphene nanoribbons. It is found that the horizontal shift of a single defect produces no changes to the conductance, while the different defect positions in vertical direction leads to different conductances and hence the center of loop current patterns. In Fig. 5(a) we choose, respectively, four sites (labeled by A, B, C, and D) as a single defect site to make a comparison. The conductance corresponding to these four choices for the defect site is plotted in Fig. 5(b). One can see that for each case the conductance drops to zero with a dip. The width of the dip becomes smaller with the site going closer to the boundary [see the inset in Fig. 5(b)]. By comparing the current flowing through these sites in perfect lattice, we see that the defect locating on the position with bigger current in the perfect lattices would cause a conductance dip with a broader width.

The role of the presence of a single defect-lattice site becomes more important in the graphene nanoribbons with armchair edges. As we know, a graphene nanoribbon with armchair edges has the zero energy gap only when the number of atoms on a zigzag edge connecting the source (or lead) is $3M-1$ ($M$ is an integer). This kind of graphene nanoribbons hence has a quantum conductance beginning from $G_0$ with increasing the electron Fermi energy. We plot the local current distribution of the system without the defect in Fig. 6(a), which clearly displays a series of well-separated paths for current flow. Each path has the same weight in current

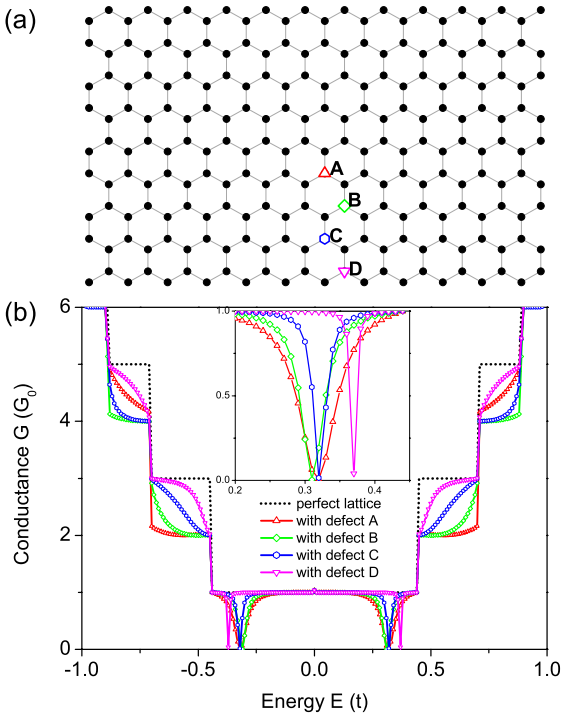


FIG. 5. (Color online) (a) The graphene nanoribbon with four different defect sites to be considered, respectively, which are labeled with A, B, C, and D. (b) Conductances of the graphene nanoribbon with one defect located at one of these four positions, respectively. Inset is the amplification of the part where the conductances drop to zero.

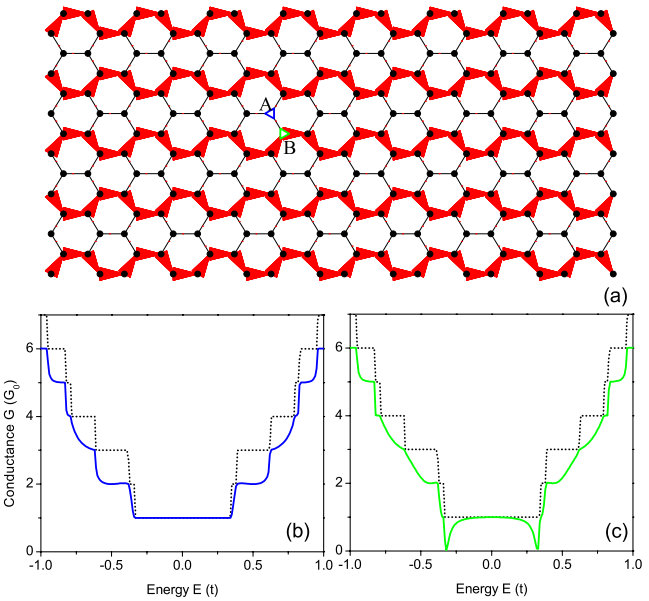


FIG. 6. (Color online) (a) Local electric current distribution (arrows) in a metallic armchair-edges graphene ribbon. Sites A (left triangle) and B (right triangle) represent two kinds of defect to be considered, respectively. (b) Conductance of the system with the defect located at position A. (c) Conductance of the system with the defect located at position B. The conductance of the system without any defect is also given with dotted lines for reference in (b) and (c).

amplitude. It is the very result of interference between the transport channels in the metallic armchair-edges graphene ribbons.[29] According to this stripe current distribution, the lattice sites in the graphene nanoribbon can be therefore classified into two parts, i.e., sites such as A [see Fig. 6(a)] carrying the current flow and sites such as B without carrying the current flow. We set the single defect site to be on site A or on site B and then calculate the corresponding quantum conductance, respectively. The results are shown in Figs. 1(b) and 6(c), respectively. Remarkably, it is shown in Fig. 6(b) that when a single defect is placed on site A, no conductance dip occurs at all and the first quantum conductance step is invariant upon the presence of the defect. Whereas, when the defect is placed on site B, two dips develop in the conductance spectrum, as shown in Fig. 6(c). Again, at the energy position $E=0.32t$ of the conductance dip, the spatial distribution of the internal current (not shown here) is featured by a loop current around the defect site. Thus, the lattice sites B are more important than the lattice sites A for the transport in this kind of armchair-edges graphene ribbons. This is an important ingredient for practical control of the graphene transport by manipulating the position of a single defect site. From the point of the interference among different transport channels mentioned above, the defect in site B gives a kind of destructive interference. The local current-density distribution pattern of the perfect metallic armchair-graphene ribbons indicates that the total conductance is mainly contributed by several parallel and independent channels. At the site A, the local density is zero. In other words, the site A is decoupled and isolated from these channels. That is why the graphene ribbon is immune to the defect on site A.

## III. CONCLUSION

In summary, we have studied the influence of a single defect on the electron-transport properties in narrow graphene nanoribbons with different edges, widths, and positions of the defect. It has been found that the conductances may drop even down to zero at certain Fermi energies in the presence of a single defect site for metallic graphene nanoribbons. The conductance dip is accompanied by the formation of a remarkable loop current around the defect. The width of the conductance dip is sensitive to the position as well as to the severity of the defect site. For the graphene nanoribbons with armchair edges, it has been found that the transport properties, including the low-energy conductance step, the conductance dip, and the loop current, can be controlled by choosing the position of the single defect. This result enlightens us in controlling the conductance of the graphene nanoribbons by simply manipulating the defects due to the absorbed atom.

*yan_jieyun@iapcm.ac.cn

[1] Y. Zhang, Y.-W. Tan, H. L. Stormer, and P. Kim, Nature (London) **438**, 201 (2005).
[2] K. S. Novoselov, Z. Jiang, Y. Zhang, S. V. Morozov, H. L. Stormer, U. Zeitler, J. C. Maan, G. S. Boebinger, P. Kim, and A. K. Geim, Science **315**, 1379 (2007).
[3] K. S. Novoselov, A. K. Geim, S. V. Morozov, D. Jiang, M. I. Katsnelson, I. V. Grigorieva, S. V. Dubonos, and A. A. Firsov, Nature (London) **438**, 197, (2005).
[4] C. L. Kane, Nature (London) **438**, 168 (2005).
[5] A. H. Castro Neto, F. Guinea, N. M. R. Peres, K. S. Novoselov, and A. K. Geim, Rev. Mod. Phys. **81**, 109 (2009).
[6] N. M. R. Peres, A. H. Castro Neto, and F. Guinea, Phys. Rev. B **73**, 195411 (2006).
[7] Z. Li, H. Qian, J. Wu, B.-L. Gu, and W. Duan, Phys. Rev. Lett. **100**, 206802 (2008).
[8] F. Munoz-Rojas, D. Jacob, J. Fernandez-Rossier, and J. J. Palacios, Phys. Rev. B **74**, 195417 (2006).
[9] P. Ruffieux, O. Gröning, P. Schwaller, L. Schlapbach, and P. Gröning, Phys. Rev. Lett. **84**, 4910 (2000).
[10] A. Hashimoto, K. Suenaga, A. Gloter, K. Urita, and S. Iijima, Nature (London) **430**, 870 (2004).
[11] P. Esquinazi, D. Spemann, R. Höhne, A. Setzer, K.-H. Han, and T. Butz, Phys. Rev. Lett. **91**, 227201 (2003).
[12] P. L. McEuen, M. Bockrath, D. H. Cobden, Y. G. Yoon, and S. G. Louie, Phys. Rev. Lett. **83**, 5098 (1999).
[13] T. Zhou, J. Wu, W. Duan, and B.-L. Gu, Phys. Rev. B **75**, 205410 (2007).
[14] H. Matsumura and T. Ando, J. Phys. Soc. Jpn. **70**, 2657 (2001).
[15] B. An, S. Fukuyama, K. Yokogawa, M. Yoshimura, M. Egashira, Y. Korai, and I. Mochida, Appl. Phys. Lett. **78**, 3696 (2001).
[16] Y.-Y. Zhang, J.-P. Hu, B. A. Bernevig, X. R. Wang, X. C. Xie, and W. M. Liu, Phys. Rev. B **78**, 155413 (2008).
[17] J. J. Palacios, J. Fernández-Rossier, and L. Brey, Phys. Rev. B **77**, 195428 (2008).
[18] P. O. Lehtinen, A. S. Foster, A. Ayuela, A. Krasheninnikov, K. Nordlund, and R. M. Nieminen, Phys. Rev. Lett. **91**, 017202 (2003).
[19] H. Sahin and R. T. Senger, Phys. Rev. B **78**, 205423 (2008).
[20] N. M. R. Peres, F. D. Klironomos, S. W. Tsai, J. R. Santos, J. M. B. Lopes dos Santos, and A. H. Castro Neto, EPL **80**, 67007 (2007).
[21] W. Long, Q. F. Sun, and J. Wang, Phys. Rev. Lett. **101**, 166806 (2008).
[22] M. T. Lusk and L. D. Carr, Phys. Rev. Lett. **100**, 175503 (2008).
[23] T. C. Li and S.-P. Lu, Phys. Rev. B **77**, 085408 (2008).
[24] S. Datta, *Electronic Transport in Mesoscopic Systems* (Cambridge University Press, Cambridge, UK, 1995).
[25] D. H. Lee and J. D. Joannopoulos, Phys. Rev. B **23**, 4997 (1981).
[26] J. Zhang, Q. W. Shi, and J. Yang, J. Chem. Phys. **120**, 7733 (2004).
[27] M. P. Anantram, M. S. Lundstrom, and D. E. Nikonov, Proc. IEEE **96**, 1511 (2008).
[28] O. V. Yazyev and L. Helm, Phys. Rev. B **75**, 125408 (2007).
[29] K. Wakabayashi, M. Fujita, H. Ajiki, and M. Sigrist, Phys. Rev. B **59**, 8271 (1999).